

# Magnetic breakdown with spin-flip: the galvanomagnetic properties of metals with small orbits (Zn)

Yu. N. Proshin, N. Kh. Useinov

*V. I. Ul'yanov-Lenin State University, Kazan*

(Received 13 March 1991)

Zh. Eksp. Teor. Fiz. **100**, 1088–1103 (September 1991)

Interband magnetic breakdown (MB) theory incorporating the spin degrees of freedom of the conduction electrons is applied to calculating the galvanomagnetic properties of metals whose electron trajectories have small triangular orbits under MB conditions. Effective MB-scattering matrices of rank six are derived for the small orbits. Expressions for the magnetoresistance and conductivity are obtained by the "effective path" method. Quantitative agreement with reported experimental data for zinc is obtained. Values for the characteristic magnetic breakdown field, the electron  $g$ -factor of the "whiskers" and the spin-orbital interaction parameter are derived from a fit of theory to experiment.

1. Conduction electron tunnelling between the trajectories of different bands in a strong magnetic field, which has come to be called "magnetic breakdown" (MB),<sup>1</sup> has been the subject of comprehensive theoretical and experimental research.<sup>2-5</sup> However, the spin of the conduction electron has only been incorporated formally in most theoretical studies, even in the most comprehensive and consistent theory of MB developed by Slutskin<sup>3b</sup> (see also the references surveyed in Ref. 3a).

A recent study<sup>6</sup> generalized Slutskin's theory<sup>3b</sup> to the case where both the conduction electron spin and the spin-orbit interaction are taken into account. This substantially modified the electron dynamics under MB conditions. Specifically, it gave rise to a spin-flip probability of the conduction electron in MB, with the magnitude of the characteristic MB field  $H_0$  renormalized due to the spin-orbit interaction. The electronic spectrum (the MB-spectrum) was also modified. Incorporation of the spin degrees of freedom of the conduction electrons therefore made it necessary to reconsider the existing theoretical interpretation of experimental data for MB metals, particularly those for which the effort of spin-orbit interaction on the formation of the band spectrum cannot be neglected.

As previously reported<sup>2-4</sup> the topology of conduction electron trajectories is modified under MB conditions: A planar network of quasiclassical regions is set up in reciprocal space; such regions belong to different bands and are interconnected by small domains (MB-nodes) where the MB-induced interband transitions of the conduction electrons occur. The incorporation of the spin-orbit interaction<sup>6</sup> combines the quasiclassical regions with different electron spin projections in a single MB-configuration. In this case motion of the conduction electrons through the MB-configuration acquires a probabilistic character with the electron wave functions of the different sections related by MB-scattering  $s$ -matrices<sup>6</sup> which can be used to calculate the MB probabilities as well as many macroscopic characteristics of MB-metals, particularly galvanomagnetic properties.<sup>2-4,7</sup>

Metals whose MB-configurations contain orbits far smaller than the reciprocal lattice constant (such as Zn, Mg, Al, Be, Sn, etc.) are of special interest. Indeed, the development of small orbits can often be attributed to small cavities

in the Fermi surface (FS) in the formation of which spin-orbit interaction commonly play a significant role.<sup>8</sup> This latter process will often cause the  $g$ -factor of the conduction electrons in such FS cavities to deviate significantly from its  $g_0$  value for free electrons.<sup>9</sup> We also know that the coherent orbital motion condition of the free electrons<sup>3a</sup>

$$\tau, \tau_{sa} \gg 1/\omega_c, \quad (1)$$

holds for these orbits with significantly less severe constraints on metal purity or temperature, compared to orbits with linear dimensions of the order of the reciprocal lattice constant ( $\omega_c$  is the characteristic cyclotron frequency,  $\tau$  is the pulse relaxation time,  $\tau_{sa}$  is the characteristic small-angle scattering time). The small size of such orbits makes it possible to treat such orbits as unique "quantum" switches controlling conduction electron motion through the MB-configuration. Coherent motion in small orbits under MB conditions will produce oscillations of the kinetic coefficients with a period corresponding to the area of the small orbit.<sup>2-7</sup> However, the theory<sup>7</sup> explaining the existence, form and order of magnitude of such oscillations has not provided a correct description of the experimentally observed double-peak structure of the oscillations in the galvanomagnetic characteristics and is not in satisfactory quantitative agreement with experiment for zinc.<sup>10</sup>

Recently it was demonstrated<sup>11</sup> for the case of a model metal with a simple MB configuration containing small "crescent" orbits that incorporating the spin degrees of freedom of the conduction electrons in calculating the magnetoresistance complicates the form of the MB-oscillations and produces a double-peak line shape.

An MB theory with possible spin-flip of the conduction electrons is developed in this paper for calculating the galvanomagnetic characteristics of a real MB-metal. Both qualitative and quantitative agreement with the experimental data for zinc<sup>10</sup> are obtained. This suggests an experimental confirmation of the MB theory with spin-flip of the conduction electron developed in Ref. 6.

The magnetoresistance and conductivity were calculated by the "effective path" method<sup>2,4,7</sup> in the limit of stochastic motion of the conduction electrons in large orbits and

coherent motion of the conduction electrons in small orbits for a two-dimensional MB-network with small “triangles” (Sec. 4) for HCP metals (Zn, Mg). The effective  $s$ -matrices and transmission probabilities were precalculated (Sec. 3) for small “triangular” orbits. The results are discussed in Sec. 5 and are compared to both experimental data and to reported theoretical results. In the following section we briefly outline the fundamental concepts of the MB theory incorporating the spin degrees of freedom.<sup>6</sup>

2. Many properties of metals are accurately described in the quasiclassical approximation.<sup>12,13</sup> In this approximation the conduction electrons in a magnetic field  $\mathbf{H}(0, 0, H)$  travel in reciprocal space along trajectories formed by the intersection of the Fermi surface and a plane perpendicular to the magnetic field:

$$\varepsilon_{n\sigma}(\mathbf{k}) = \varepsilon_F, \quad k_z = k_{z0} = \text{const}; \quad (2)$$

here  $n$  is the band number,  $\sigma = \uparrow, \downarrow$  is the “spin” index indicating the effect of spin-orbit interaction,<sup>8</sup>  $\varepsilon_F$  is the Fermi energy,  $k$  is the wave vector, and  $\varepsilon_{n\sigma}(k)$  gives the dispersion law of the conduction electrons.

After solving the corresponding Schrödinger equation in the MB domain, Proshin<sup>6</sup> determined that incorporation of spin-orbit interaction causes the principal dynamical characteristic of MB—the  $s$ -matrix—to become a  $4 \times 4$  matrix, which describes the three-channel scattering of the conduction electron under MB, including MB with spin-flip. In this case, each quasiclassical segment of trajectory (2) can be characterized by the set  $i\sigma$ , where  $i$  is the “zero-spin” number (henceforth, simply the segment number), and  $\sigma$  defines the spin direction of the conduction electron along the trajectory. The band number  $n$  is unambiguously determined by the segment number  $i$ . In this case, the unitary  $s$ -matrix relates at the MB-node the amplitudes  $c_{i\sigma}$  of the eight quasiclassical wave functions  $\psi_{i\sigma}$  of the conduction electrons of the two bands undergoing breakdown before and after MB-scattering:

$$c_{i\sigma} = \sum_{i'\sigma'} s_{i\sigma, i'\sigma'} c_{i'\sigma'}. \quad (3)$$

A schematic representation of the MB-node is shown in Fig. 1. The primes in Eq. (3) and the figures label the numbers of the outgoing quasiclassical segments from the MB-node, together with the corresponding electron spin projections; the unprimed designations apply to the incoming trajectory segments;  $s_{i\sigma, i'\sigma'}$  is the matrix element of the  $s$ -matrix expressed in terms of the dispersion law at the “maximum-breakdown” point  $k_M$  and written as

$$s = \begin{bmatrix} \tau \exp(-i\Lambda) & 0 & \rho/\beta & \alpha\rho/\beta \\ 0 & \tau \exp(-i\Lambda) & -\alpha\rho/\beta & \rho/\beta \\ -\rho/\beta & \alpha\rho/\beta & \tau \exp(i\Lambda) & 0 \\ -\alpha\rho/\beta & -\rho/\beta & 0 & \tau \exp(i\Lambda) \end{bmatrix}, \quad (4)$$

$$\rho^2 = \exp(-H_0/H), \quad \tau^2 + \rho^2 = 1, \quad \beta = (1 + \alpha^2)^{1/2}. \quad (4a)$$

Here  $\rho, \tau, \Lambda$  are real functions of  $H, H_0, \varepsilon_F, k_z$ . The function

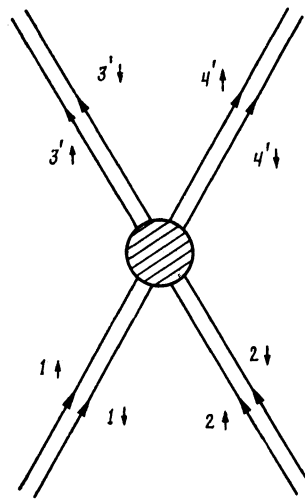


FIG. 1. Schematic representation of an MB node (1, 2: Incoming segments of quasiclassical trajectories; 3', 4': Outgoing segments). The arrows indicate the direction of motion of the conduction electron and the spin direction  $\sigma$ .

$$\Lambda = \left[ \frac{\pi}{4} + \frac{H_0}{\pi H} + \arg \Gamma \left( i \frac{H_0}{\pi H} \right) - \frac{H_0}{\pi H} \ln \frac{H_0}{\pi H} \right] \times \text{sign} [ \varepsilon_{n(i)}(\mathbf{k}_M) - \varepsilon_{n(i')}(\mathbf{k}_M) ] \quad (4b)$$

defines the phase jump of the wave function of the conduction electrons under MB. Numerical analysis of these results requires that the argument of the gamma-function be written in terms of elementary functions. From Ref. 14 we easily obtain ( $\text{Im } y = 0$ )

$$\arg \Gamma(iy) = -Cy - \frac{\pi}{2} + \sum_{n=1}^{\infty} \left( \frac{y}{n} - \text{arctg} \frac{y}{n} \right), \quad (4c)$$

where  $H_0$  and  $\alpha$  are the characteristic MB field and the spin-orbit interaction parameter in MB theory, respectively. Their exact form is provided in Ref. 6.<sup>1</sup> We merely note that  $H_0$  is renormalized from the spin-orbit interaction:  $H_0 = H_0^0/\beta$ , where  $H_0^0$  is the characteristic MB field neglecting the spin-orbit interaction ( $\alpha = 0, \beta = 1$ ) which coincides with the reported value.<sup>2</sup> An estimate of  $\alpha$  demonstrates that when the effect of the spin-orbit interaction is strong,  $\alpha$  is of order unity, while with weak spin-orbit interaction  $0 \leq \alpha < 1$  (Ref. 6).

The stationary state of conduction electrons under MB conditions is described by the general wave function

$$\Psi = \sum_{i\sigma} c_{i\sigma} \psi_{i\sigma}(k_v) \delta_{k_z, k_{z0}}, \quad (5)$$

which is a superposition of the wave functions of the individual segments whose exact form is reported in Ref. 6 taking the spin of conduction electrons into account. Summation is carried out over  $i$  in Eq. (5) through  $N$ , the total number of nonequivalent segments in the MB-configuration. Figure 2 shows a schematic representation of certain MB-configurations. Under coherent MB conditions<sup>3a</sup> when the phase of the wave function remains unchanged from the motion of conduction electrons through MB-configuration (1) the single-valuedness (and the periodicity in the case of open and periodic MB-configurations) requirement imposes the following constraint on the amplitudes  $c_{i\sigma}$  of the wave functions<sup>3,6</sup>:

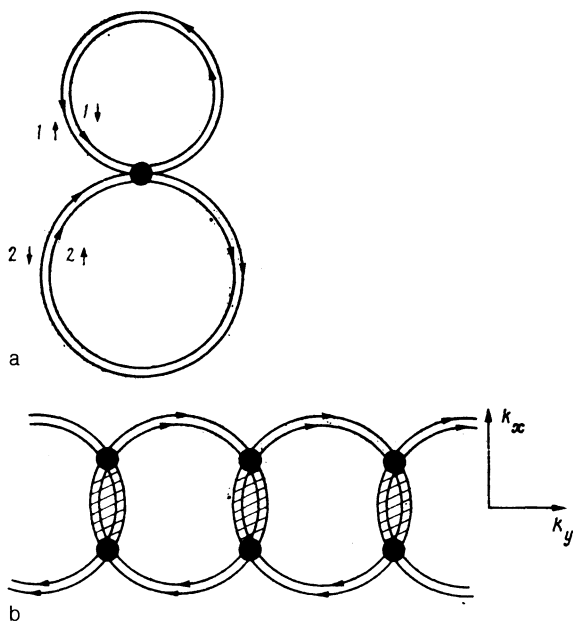


FIG. 2. MB configurations taking account of the spin degrees of freedom: a—Closed MB configuration ( $i = 1, 2$  are the segment numbers) with a single MB node; b—open MB configuration that is periodic in the  $k$ -space with small "crescent" orbits. The solid circles represent MB nodes, while the shaded regions denote the effective MB nodes.

$$c_{i\sigma} - \sum_{j\sigma'} V_{i\sigma, j\sigma'}^0 \exp(i\gamma_{j\sigma'}) c_{j\sigma'} = 0. \quad (6)$$

Here  $\hat{V}^0$  is a unitary matrix of rank  $2N$  with only three non-zero elements in each  $j\sigma'$ th column. These elements are in the rows  $i\sigma$  whose numbers are identical to those of the segments connected to segment  $j\sigma'$  by the common node

$$V_{i\sigma, j\sigma'}^0 = s_{i\sigma, j\sigma'}^0, \quad (7)$$

where  $\hat{s}^0$  is obtained from Eq. (4) if we set all  $\Lambda$  equal to 0. Note that the spectrum of the conduction electrons under MB conditions (the MB-spectrum) is obtained from the vanishing of the determinant of the system (6). The phase  $\gamma_{i\sigma}$  for closed MB-configurations appears as<sup>6</sup>

$$\gamma_{i\sigma}(\varepsilon_F, k_z) = \varphi_{i\sigma} + (\Lambda_{\bar{i}} + \Lambda_i)/2, \quad (8)$$

where

$$\varphi_{i\sigma}(\varepsilon_F, k_z) = S_i/\hbar + \gamma_{i\sigma}^0 + \delta_i \quad (9)$$

is the quasiclassical phase of the wave function  $\psi_{i\sigma}$  acquired by the conduction electron on the  $i\sigma$ -segment between two successive MB-scattering events;  $S_i(\varepsilon_F, k_z)$  is the transverse increment neglecting conduction electron spin;  $\bar{i}$  is the number of the segment into the MB-node from which the  $i$  segment originates, where  $n(\bar{i}) = n(i)$ ;  $\delta_i = \pm \pi/2$  is the sum of all phase jumps in the  $i$ -segment through the classical turning points; and the spin contribution to phase  $\gamma_i^0$  is determined by the relation<sup>6</sup>

$$\gamma_i^0(\varepsilon_F, k_z) = \pm \frac{1}{2\hbar} g_i \mu_B H T_i = \pm \frac{1}{2} \pi g_i \frac{m_{ci}}{m_0}. \quad (10)$$

Here  $g_i(\varepsilon_F, k_z)$ ,  $m_{ci}(\varepsilon_F, k_z)$  is the  $g$ -factor and the effective cyclotron mass of the conduction electron in the  $i$ -segment,

$T_i(\varepsilon_F, k_z)$  is the transit time of the conduction electron across the  $i$ -section;  $\mu_B$  is the Bohr magneton. Here and below the upper sign in Eq. (10) corresponds to  $\sigma = \uparrow$  while the lower sign corresponds to  $\sigma = \downarrow$ .

The motion of the conduction electron (the quasiclassical wave packet<sup>3a</sup>) along the MB-configuration can be represented as follows.<sup>3a,6</sup> The conduction electron follows the quasiclassical segment of trajectory (2), acquiring a phase in accordance with Eq. (9), through the nearest MB-node, after which it has different probabilities of appearing on different outgoing segments from the MB-node. The tunnelling probabilities to a segment of a different band are determined by the square of the absolute value of the corresponding non-diagonal elements of the  $s$ -matrix describing this MB-node, while the probability of remaining in its band is determined by the diagonal elements. Specifically, the probability of MB with spin-flip of the conduction electron takes the following form:

$$w_s = |s_{1,2}|^2 = \frac{\alpha^2}{1+\alpha^2} \exp\left(-\frac{H_0}{H}\right). \quad (11)$$

The energy spectrum and macroscopic characteristics of the metal under MB conditions are expressed in terms of the  $s$ -matrix. The phases acquired by the conduction electrons on the equivalent segments can be differentiated by small angle scattering with zero interference<sup>3</sup> in the case of stochastic MB ( $\tau \gg 1/\omega_c \gg \tau_{sa}$ ); mathematically this is described by phase-averaging the results obtained for the case of coherent MB.<sup>4,15</sup>

3. The Fermi surface of HCP metallic zinc is well-known.<sup>16</sup> The following parts of the Fermi surface interconnected under MB will be important in our analysis: The "hole monster" in the second band with characteristic dimensions comparable to those of the Brillouin zone, and six small electron cavities ("needles" in the third band along the vertical edges of the Brillouin zone). A schematic representation of the MB-configuration obtained for the case where the magnetic field  $\mathbf{H}$  runs along the axis of symmetry of a sixth order crystal is shown in Fig. 3 (neglecting the spin

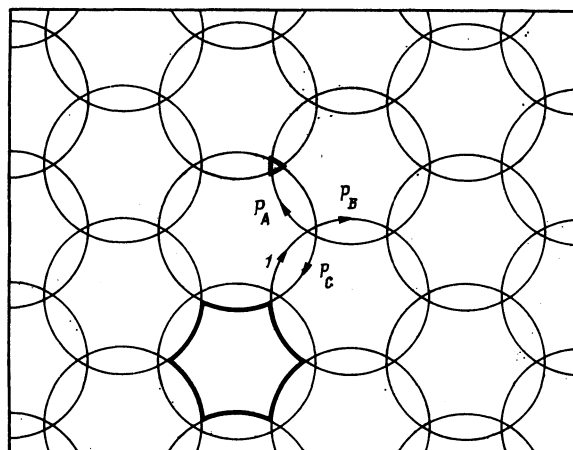


FIG. 3. Schematic representation of the cross section of the Fermi surface of Zn in the plane  $k_z = 0$  (the  $z$  axis is parallel to the hexagonal axis), which forms the MB configuration with small triangular orbits from the "whiskers" and large orbits from the "monster" (bold);  $P_A, P_B, P_C$  are the effective MB probabilities.

degrees of freedom for purposes of simplicity). This MB-configuration contains small "triangular" orbits. The characteristic cyclotron frequency of such a small orbit  $\omega_c^m$  is far greater than the cyclotron frequency of a large orbit  $\omega_c^0$  which in this case applies to the "monster" conduction electrons. The coherence condition (1) in this case can be transformed to

$$\tau > 1/\omega_c^0 \gg \tau_{sa} \gg 1/\omega_c^m, \quad (12)$$

i.e., the conduction electrons travel stochastically along the large segments of the MB-configuration (the phase of their wave function wanders!) while the conduction electrons travel coherently along small orbits. This corresponds to the actual case of the intermediate MB state. Since the "triangles" are also substantially smaller than the "monster",<sup>7,10</sup> this MB-network can be replaced by a reduced MB-configuration in which effective MB-nodes (Fig. 4), described by effective  $s$ -matrices  $\hat{s}^{\text{eff}}$ , are substituted for all small orbits.

In our case the unitary matrix  $\hat{s}^{\text{eff}}$  has a rank of six including the spin degrees of freedom. The expression for its matrix elements can be obtained from the general system (6) by eliminating from this system the amplitudes  $c_{k\eta}$  applying to the small orbit sections  $k\eta$  (for the "zero-spin" case this procedure is described in Ref. 3a for a matrix of rank three):

$$S_{i\sigma, j'\sigma'} = \sum_{\lambda} a_{i\sigma, j'\sigma'}^{\lambda} \exp[i\gamma^{\lambda}(\epsilon_F, k_z)]. \quad (13)$$

Here  $i\sigma$  ( $j'\sigma'$ ) are the numbers and projections of the electron spins of the large orbit segments interconnected by a small orbit (Fig. 4). Summation is carried out over all possible  $\lambda$ -paths in Eq. (13) (Ref. 3a) that connect the incoming segment  $i\sigma$  to the outgoing segment  $j'\sigma'$ , passing only through the MB-nodes of the small orbit.

The structure of the  $s$ -matrix (4) is such  $s_{i\sigma, j'\sigma'} = s_{j'\sigma', i\sigma} \equiv 0$ ) that there will be no MB-induced spin-flip of the conduction electron as it travels along the small orbit. A spin-flip is possible only upon entering or exiting a small

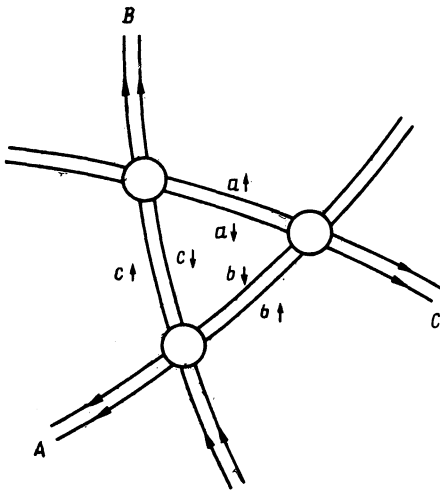


FIG. 4. The effective MB node from a small "triangular" orbit taking account of the spin degrees of freedom. This node connects the large segments A, B, C via the small segments a, b, c. The arrows indicate the direction of the conduction electron and the spin  $\sigma$ .

orbit. It is therefore clear that there are only two possible sets of  $\lambda$ -paths for any small orbit with arbitrary  $i\sigma$  and  $j'\sigma'$ : A conduction electron can traverse a small orbit either with an up or a down spin. Within each set, the  $\lambda$ -paths differ from one another only by the number  $r$  of revolutions along the small orbit, i.e. (see Fig. 4), by either  $(a_1 - b_1 - c_1)^r$  or by  $(a_1 - b_1 - c_1)^r$ . Therefore, each  $\lambda$ -path is determined by the numbers of the incoming and outgoing segments of the large orbits ( $i$  and  $j'$ ), the spin state of the small orbit  $\eta$  and the number of revolutions  $r$ .

In Eq. (13)  $a_{i\sigma, j'\sigma'}^{\lambda}$  is the product of the corresponding matrix elements of the  $s$ -matrices  $\hat{s}^0$  of all MB-nodes encountered on the given  $\lambda$ -path. For example, for the symmetrical case when all MB-nodes of a "triangular" orbit are equivalent

$$a_{1\uparrow, 2'\uparrow}^{\lambda_1} = \frac{\rho^2 \tau^r}{1 + \alpha^2}, \quad a_{1\uparrow, 2'\uparrow}^{\lambda_2} = \frac{\alpha^2 \rho^2 \tau^r}{1 + \alpha^2},$$

where  $\alpha$ ,  $\rho$  and  $\tau$  are determined by Eqs. (4) and (4a).

The phase  $\gamma^{\lambda}(\epsilon_F, k_z)$  acquired by the conduction electron on the  $\lambda$ -path is determined by Eqs. (8)–(10), which require the following redesignation:  $\gamma_{i\sigma} \rightarrow \gamma^{\lambda}$ ,  $\lambda = \lambda(i, j', \eta, r)$ ; then

$$\gamma^{\lambda} = \tilde{\gamma}_{ij}^{\eta} + r\gamma_{m\eta},$$

where

$$\gamma_{m\eta} = \frac{c\hbar}{eH} A_m + \gamma_{m\eta}^s + \frac{1}{2} \sum_k (\Lambda_k + \Lambda_k^-) \quad (14)$$

is the phase acquired by the conduction electron in a single revolution on the small orbit ( $k$  adopts the three values  $a, b, c$ ; see Fig. 4). Here

$$A_m(\epsilon_F, k_z) = -\frac{eH}{c\hbar^2} \sum_k S_k(\epsilon_F, k_z)$$

is the "zero-spin" area of the small orbit; the spin contribution  $\gamma_{m\eta}^s$  is determined by Eq. (10) with  $i$  substituted for  $m$  to denote that it belongs to the entire small orbit;  $\tilde{\gamma}_{ij}^{\eta}$  is the incomplete phase (8) acquired during electron motion along the segments of the small orbit; for  $j = i$  (Fig. 4) we have  $\tilde{\gamma}_{ii}^{\eta} = \gamma_{m\eta}$ .

In the general case, when we assume that conduction electrons travelling along different segments of the small orbit acquire different phases, while the MB-nodes connecting such segments are treated as nonequivalent nodes, the expression for the effective  $s$ -matrix becomes cumbersome and of little use. We therefore only provide results for the symmetrical case when  $\gamma_{a\eta} = \gamma_{b\eta} = \gamma_{c\eta}$ , where all three MB-nodes are treated as equivalent (see the Appendix). This also corresponds to the Zn case for which the experiment was conducted.<sup>10</sup>

Our calculation of the galvanomagnetic characteristics of MB-metals will require the effective probabilities of the conduction electrons traversing the small orbits (the effective MB-node). Thus, a conduction electron approaching a small orbit along a "large" quasiclassical segment with a specific spin  $\sigma$  will have probabilities of traversing the orbit ( $P_B$  and  $P_C$ ) or reflection off the orbit  $P_A$  both with

( $\sigma' = -\sigma$ ) and without ( $\sigma' = \sigma$ ) a spin flip. The probabilities  $P_A^{\sigma\sigma'}$ ,  $P_B^{\sigma\sigma'}$ , and  $P_C^{\sigma\sigma'}$  are defined by the square of the absolute values of the corresponding matrix elements  $\tilde{S}^{\text{eff}}$  (A2) in a manner analogous to Eq. (11).

4. It is convenient to use the "effective path" method initially developed in Refs. 7, 17 and discussed in detail in Ref. 4 to calculate the galvanomagnetic characteristics of zinc which has a two-dimensional MB-network with small orbits. Slutskin's indisputably more general approach<sup>18</sup> based on a consistent derivation of kinetic equations has not, unfortunately, been developed for the quantitative analysis of two-dimensional MB-configurations.<sup>3a</sup>

We generalize the effective-path method to the case of the probability of MB with a spin-flip (spin-orbit interaction taken into account,  $\alpha \neq 0$ ) and spin-splitting ( $g_m \neq 0$ ) for the intermediate MB-state defined by condition (12). In this analysis we make the natural assumption for pure metals and low temperatures that the characteristic spin relaxation time  $\tau_s$  is much greater than any other time characterizing the problem ( $\tau, \tau_{sa}, \omega_c^{-1}$ ).

In the conduction calculation, the electron is treated as a charge carrier. Hence, neglecting coherent effects on large orbits, the total probabilities of traversing the orbit or reflection off the orbit are important for a conduction electron approaching a small orbit with a specific spin  $\sigma$  (see Figs. 3 and 4):

$$P_K^\sigma = \sum_{\sigma'} P_K^{\sigma\sigma'}, \quad K=A, B, C,$$

where

$$P_A^\sigma = 1 - P_B^\sigma - P_C^\sigma, \quad P_C^\sigma = \tau^2 P_B^\sigma, \quad (15)$$

$$P_B^\sigma = \frac{(1-\tau^2)^2}{1+\alpha^2} \sum_{\eta} |\Gamma_{\eta}|^2 (\delta_{\sigma,\eta} + \alpha^2 (1-\delta_{\sigma,\eta})), \quad (16)$$

using the notation of Eq. (A1) it is easily determined that

$$|\Gamma_{\eta}|^2 = |\Gamma_{i\eta'}|^2 = \frac{1}{1+\tau^6 - 2\tau^3 \cos \gamma_{m\eta}}. \quad (16a)$$

The results from the effective-path method<sup>7,17</sup> are easily written out by means of the complex coordinate  $x + iy$ . In this case the conductivity takes the form

$$\hat{\sigma} = \sigma_{xx} - i\sigma_{yx} = \sigma_{11} - i\sigma_{21}, \quad \sigma_{12} = -\sigma_{21}. \quad (17)$$

Since the layer of MB-configurations along  $k_z$  has a finite thickness  $2k_{zm}$ , while the parameters of the MB and the cross-sectional area of the small orbit  $A_m$  are generally functions of  $k_z$ , the expression for the conductivity tensor  $\hat{\sigma}$  can be written as an integral:<sup>7</sup>

$$\sigma_\sigma = \frac{1}{H} \int_{-k_{zm}}^{k_{zm}} \frac{3nec}{\pi} \bar{D}_\sigma(k_z) dk_z + \frac{a}{H^2}, \quad (18)$$

$$\bar{D}_\sigma(k_z) = \xi^2 + \frac{\xi}{1-3^{1/2}iP_B^\sigma(\xi+\tau^2)} + 3^{1/2}i. \quad (18a)$$

Here we have written  $\xi = \exp(-i\pi/3)$  and  $n(k_z)dk_z$  defines electron density per unit volume in the elementary FS

cross-section;  $a$  is an empirical parameter. Unlike Ref. 7, the spin index was used in Eq. (18).

In the absence of MB all electron orbits (2) are closed, and they make the primary contribution to  $\sigma_{xx} \sim a/H^2$  for  $\omega_c \tau \gg 1$  (Refs. 12, 13). The second term in Eq. (18) therefore describes the contribution to the conductivity from all closed orbits outside the MB-layer. The resulting narrow layer of open MB-configurations ( $k_{zm} \approx 0.04k_F$  for zinc<sup>2</sup>) is accounted for by the first term in Eq. (18). It is this term that makes the dominant contribution to the galvanomagnetic characteristics in the case of well developed MB ( $H \gg H_0$ ). In the limiting case of vanishing MB,  $\sigma_{xy} \rightarrow 0$ , i.e., for  $H \ll H_0$ , the metal is completely compensated.

The expression for the total conductivity  $\hat{\sigma}$  is obtained after averaging Eq. (18) over the initial spin states (an analogous procedure is used in calculating the Kondo effect<sup>13</sup>):

$$\hat{\sigma} = \frac{1}{2} \sum_{\sigma} \hat{\sigma}_\sigma. \quad (19)$$

In the general case,  $\hat{\sigma}$  in Eqs. (18) and (19) depends on the magnetic field  $H$ ; the microscopic parameters of the MB nodes (the characteristic MB field  $H_0$  and the spin-orbit interaction parameter  $\alpha$ ); the characteristics of the small orbit (the "zero-spin" area  $A_m$ , the  $g$ -factor  $g_m$ , and the cyclotron mass  $m_{cm}$ ); and the thickness of the MB-layer  $2k_{zm}$  and the fitting parameter  $a$ . Estimates suggest that the area of the "triangle" has the strongest dependence on  $k_z$  in the integrand

$$A(k_z) = A_0 + \xi k_z^2, \quad (20)$$

where  $A_0$  is the extremal cross-sectional area of the whisker for  $k_z = 0$ ; the whisker tapering parameter

$$\xi = 1/2 (\partial^2 A / \partial k_z^2) |_{k_z=0}$$

was estimated from a variety of theoretical models. References 2 and 7 report the following estimates for  $\xi$ :  $\xi_1 = -1.13 \cdot 10^{-2}$  a.u. and  $\xi_2 = -1.77 \cdot 10^{-2}$  a.u.

Note that the integrand in Eq. (18) has a periodic dependence on the phase  $\gamma_{m\eta}(k_z)$  in Eq. (14). If the conduction electron were to manifest stochastic behavior along the small orbit ( $\omega_c^m < \tau_{sa}^{-1}$ ), this would induce stochastic behavior of the phase  $\gamma_{m\eta}$  in Eq. (18). It is therefore possible to obtain the result in the limit of stochastic MB (see, for example, Ref. 15) by averaging Eqs. (18) and (19) over this phase.

We average  $\hat{\sigma}H$  to compare these results to the reported experimental data:

$$\langle \hat{\sigma}H \rangle_{\gamma_{m\eta}} = b \langle \bar{D} \rangle_{\gamma_{m\eta}} + a/H, \quad (21)$$

$$\bar{D}(\gamma_{m\eta}(k_z)) = \frac{1}{2} \sum_{\sigma} \bar{D}_\sigma(\gamma_{m\eta}(k_z)), \quad (21a)$$

where  $\langle \dots \rangle_\gamma$  represents phase-averaging;  $\hat{D}_\sigma[\gamma_{m\eta}(k_z)]$  is determined by Eq. (18) accounting for Eqs. (16) and (16a), while

$$b = \int_0^{k_{zm}} \frac{6nec}{\pi} dk_z. \quad (22)$$

Allowing for the fact that  $6nec/\pi$  changes slowly with  $k_z$ , we can write

$$\delta H = \frac{b}{k_{zm}} \int_0^{k_{zm}} \hat{D}(k_z) dk_z + \frac{a}{H}. \quad (23)$$

The components of conductivity tensor  $\hat{\sigma}$  are determined by the components of the tensor  $\hat{D}$  in Eq. (23). Using Eqs. (21a), (18a), (16) and (16a), we find

$$D_{11} = \frac{1}{4} \sum_n \frac{1+3|\Gamma_n|^2 \tau^2}{1-3|\Gamma_n|^2 + 3|\Gamma_n|^4(1+\tau^2+\tau^4)} - \frac{1}{2},$$

$$D_{12} = -\frac{3^{1/2}}{4} \sum_n \frac{1-|\Gamma_n|^2(2+\tau^2)}{1-3|\Gamma_n|^2 + 3|\Gamma_n|^4(1+\tau^2+\tau^4)} + \frac{3^{1/2}}{2}. \quad (24)$$

Obtaining  $\hat{\sigma}$  from Eq. (23), we easily find the components of the resistance tensor:

$$\rho_{11} = \sigma_{11}/(\sigma_{11}^2 + \sigma_{12}^2), \quad \rho_{12} = \sigma_{12}/(\sigma_{11}^2 + \sigma_{12}^2). \quad (25)$$

5. In this section we discuss our results and compare these results to reported experimental<sup>10</sup> and theoretical<sup>7</sup> data. The technique for calculating the galvanomagnetic characteristics of zinc from the equations derived in the preceding section reduces to determining the parameters of the theoretical model, comparing such parameters to known values, and deriving the theoretical dependence of the unknowns on the external magnetic field  $H$ .

This process is most easily carried out in two stages. We initially find the empirical parameter  $a$  and the parameter  $b$  for Eq. (22) from the nonoscillating functions  $\langle \sigma_{11} H \rangle_\gamma$  and  $\langle \sigma_{12} H \rangle_\gamma$  (21) and then determine the optimum values of the microscopic parameters of the problem  $H_0^0$ ,  $\alpha$ ,  $A_0$  [see the

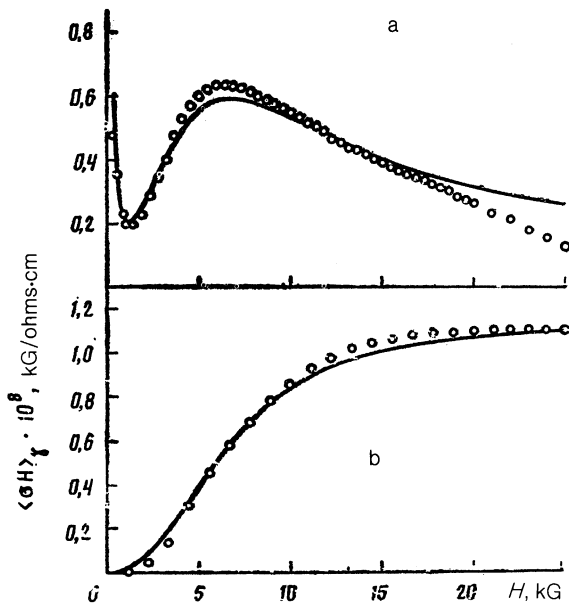


FIG. 5. Theoretical and experimental (circles) relations of the averaged quantities  $\langle \sigma H \rangle_\gamma$ : a—The diagonal component of the conductivity tensor  $\langle \sigma_{11} H \rangle_\gamma = \langle S_{22} H \rangle_\gamma$ ; b—the nondiagonal component  $\langle \sigma_{12} H \rangle_\gamma = -\langle \sigma_{21} H \rangle_\gamma$ . The experimental points are taken from curves reported in Ref. 7. The table lists the parameter values used in the derivation of the theoretical curves.

discussion of Eqs. (18), (19)] and the spin parameter  $\tilde{g} = g_m m_{cm}/2m_0$  from a fit of the theoretical and experimental galvanomagnetic oscillating characteristics. A least-squares computer fit of the theoretical curves to the experimental data was used in this case; the simplex method was employed to identify the optimum parameter values.<sup>2)</sup> The results of this procedure are shown in Figs. 5–8, while the resulting parameters are compared to previously reported values in the table.

The theoretical relations  $\langle \sigma_{11} H \rangle$  and  $\langle \sigma_{12} H \rangle_\gamma$  (21) were fitted to the experimental data over a broad range of  $H_0^0$  (2–6 kG). We found from  $\langle \sigma_{12} H \rangle_\gamma$  that the value of  $b$  characterizing the electron and hole disbalance resulting from MB lies in the range  $(0.67-0.695) \cdot 10^8 \text{ kG}/\Omega \cdot \text{cm}$ . Equation (22) can then be used to derive an “experimental” estimate of the half-width of the magnetic breakdown waist of the “whiskers”  $k_{zm}^{ex} \approx (1.8-1.9) \cdot 10^{-2} \text{ a.u.}$ : This is close to the theoretical estimate of the half-width of the waist around the midsection of the “monster”  $k_{zm}^{th} \approx 1.95 \cdot 10^{-2} \text{ a.u.}$  (Ref. 7). This agreement supports the model used here.

The next step is to find a possible value of the empirical parameter from a fit of the theoretical and experimental values  $\langle \sigma_{11} H \rangle_\gamma$ :  $a = (0.17 - 0.14) \cdot 10^8 \text{ kG}^2/\Omega \cdot \text{cm}$ .

The oscillating characteristics determined by Eqs. (23) and (25) for the conductivity and the resistance, respectively, were also numerically calculated. Note that the integral

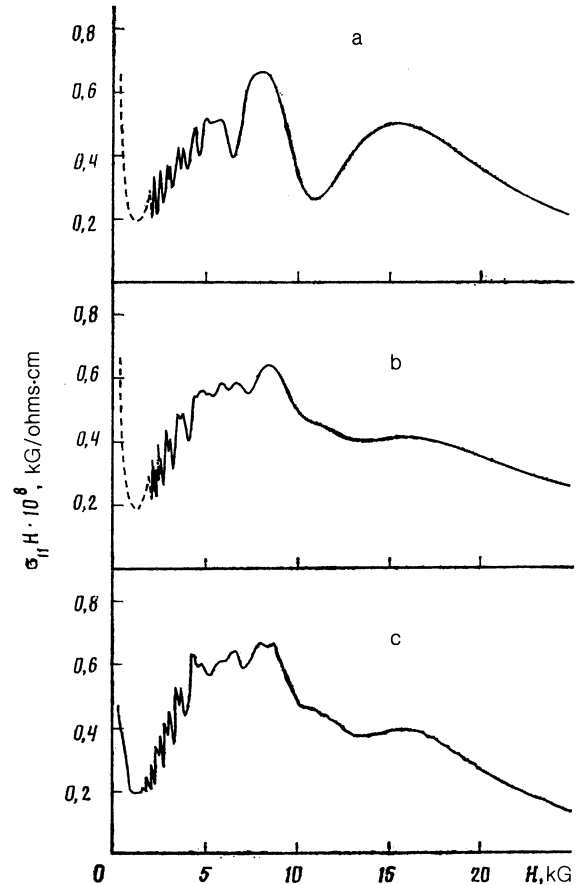


FIG. 6. Plots of oscillations in the diagonal component of the conductivity tensor  $\sigma_{11} H$  in Zn: a—Results from Ref. 7; b—our results; c—experimental curve from Ref. 7. The parameters used to derive these curves are listed in the table.

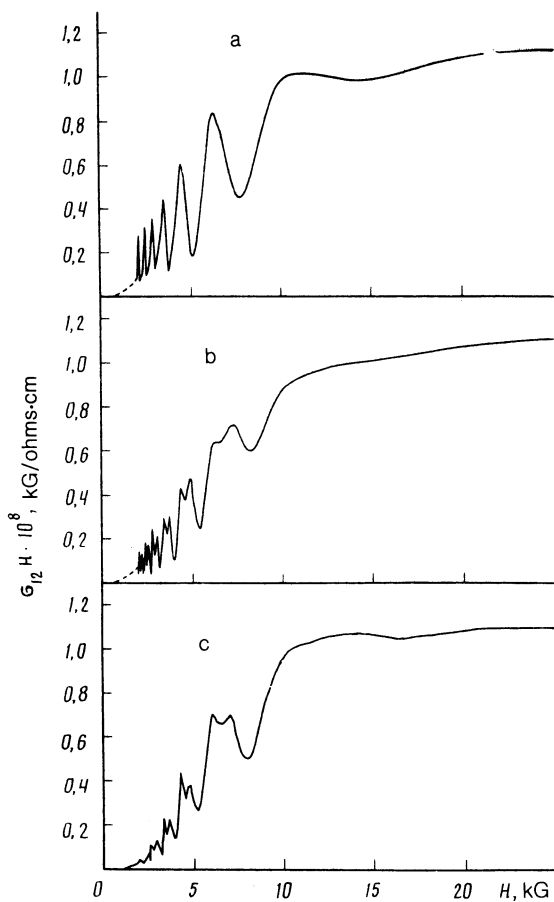


FIG. 7. Plots of the oscillations of the nondiagonal component of the conductivity tensor  $\sigma_{12}H$  in Zn: a—Results from Ref. 7; b—our results; c—experimental curve from Ref. 7. The parameter values used in plotting these curves correspond to Fig. 6.

with respect to  $k_z$  resulting from the calculation of  $\delta H$  was calculated by simple summation in Ref. 7. In this case, the interval  $0 < k_z < k_{zm}$  was divided into 20 equally spaced layers. As our calculations demonstrated, such a procedure for evaluating the integral (23) leads to errors of order 20–40%. We used one of the modifications of Simpson's method for the numerical integration (relative error of less than 1%; there were as many as 320 layers in this case for small  $H < H_0$ ).

Our theoretical curves are given in Figs. 5–8 together with existing results. The calculation parameters  $H_0^0$ ,  $\tilde{g}$ ,  $\alpha$  and  $A_0$  are listed in the table.

Naturally the results reported by Falikov, Pippard and Sievert<sup>7</sup> can be obtained from our equations if the following modifications are made:

a) Set  $\alpha = 0$ , i.e., assume spin-orbit interaction has no effect on MB.

b) Delete the dependence on the conduction electron-spin in all equations, i.e., drop the spin index uniformly and do not sum over the spin. In this case the conductivity will be calculated from Eq. (18).

c) Modify the phase (14) acquired by the conduction electron in its revolution along the small orbit:

$$\gamma_{m\eta} \rightarrow \gamma_m^{FPS} = \frac{c\hbar}{eH} A_m(k_z) + \gamma_0,$$

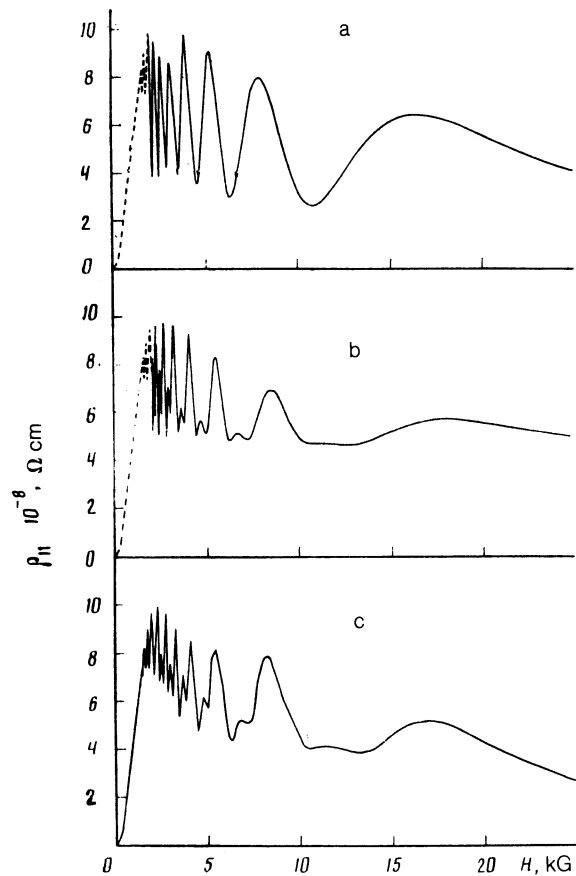


FIG. 8. Plots of the oscillations in the magnetoresistance  $\rho_{11} = \rho_{22}$  in Zn obtained by inversion of the conductivity tensor. The curves correspond to Figs. 6, 7. The parameters used in plotting the theoretical curves are listed in the table.

where  $\gamma_0 = -3.84$  is the magnetic field-independent parameter introduced into the theory by the authors of Ref. 7 to improve the fit to experiment (see Figs. 5–8) and which they used to estimate the  $g$ -factor of the conduction electrons  $\tilde{g}$  of the whisker (see table).

Since the spin contribution to phase (14) is determined accurate to  $2\pi n$  ( $n$  is an integer), it is possible to estimate the  $g$ -factor of the conduction electrons of the whisker from our value of  $\tilde{g}$ , if we know  $m_{cm}/m_0 = 0.0075$  (Refs. 4, 7):  $g_m \approx 1009 + 642n$ . Accounting for the theoretical limit on  $g_m < 266$  (Refs. 19, 20), we obtain  $g_m \approx 109$ , which is in agreement with the estimates reported in Refs. 4, 20.

We emphasize that when spin-orbit interaction is taken into account this will increase the interband gap value estimated from  $H_0^0$  by a factor of  $(1 + \alpha^2)^{1/4} = 1.1$  [see the discussion following Eq. (4c) and footnote 1].

The value of the characteristic breakdown field  $H_0$  that is dependent on the spin-orbit interaction parameter  $\alpha$  is listed in the table and is in agreement with the experimental data reported in Ref. 21.

These graphs demonstrate that the consistent theory of MB accounting for spin-flip not only provides a far better explanation of the behavior of the experimental curves (the fine structure appearing as a double-peaked structure), but also has a quantitative agreement with experiment that is quite appealing for such complicated oscillating functions. This also suggests that the intermediate MB state is observed

TABLE I.

Calculation parameters	Study [7]	Present study	Calculation parameters	Study [7]	Present study
$a \cdot 10^8$ , kG <sup>2</sup> /ohms·cm	0,17	0,17	$k_{zm}^{ex} \cdot 10^{-2}$ , a.u.	2,0	1,8
$b \cdot 10^8$ , kG <sup>2</sup> /ohms·cm	0,67	0,67	$\zeta \cdot 10^{-2}$ , a.u.	-1,77	-1,13
$H_0$ ( $H_0^0$ ), kG	2,7 (-)	3,0 (3,7)	$g$	-1,22	0,41
$A_0 \cdot 10^{-8}$ , a.u.	4,24	4,05	$\alpha$	—	0,75

under these experimental conditions.<sup>10</sup> Indeed, accounting for partial stochastization of conduction electron motion along the small orbits flattens out the sharp peaks of the MB-oscillations,<sup>15</sup> while in the case of complete stochastic MB, as we have seen (Fig. 5), the oscillations vanish altogether.

The authors wish to express their gratitude to B. I. Kochelaev and M. I. Kaganov for their interest and support in this study and to L. M. Falicov for offprints of the author's work.

## APPENDIX

We introduce the designation

$$\Gamma_{i,j'}^n = \exp(i\tilde{\gamma}_{i,j'}) [1 - \tau^3 \exp(i\gamma_{mn})]^{-1}, \quad (\text{A1})$$

then the elements of the first column of the effective  $s$ -matrix take the form

$$S_{i_1, i_1'}^{eff} = \tau^2 e^{-i\Lambda} \left[ \frac{1}{\tau} - \frac{\rho^2}{1 + \alpha^2} (\Gamma_{i_1, i_1'}^\dagger + \alpha^2 \Gamma_{i_1, i_1'}^\dagger) \right],$$

$$S_{i_1, i_1'}^{eff} = \tau e^{-i\Lambda} \frac{\alpha \rho^2}{1 + \alpha^2} (\Gamma_{i_1, i_1'}^\dagger - \Gamma_{i_1, i_1'}^\dagger),$$

$$S_{i_1, i_2'}^{eff} = - \frac{\rho^2}{1 + \alpha^2} (\Gamma_{i_1, i_2'}^\dagger + \alpha^2 \Gamma_{i_1, i_2'}^\dagger),$$

$$S_{i_1, i_2'}^{eff} = \frac{\alpha \rho^2}{1 + \alpha^2} (\Gamma_{i_1, i_2'}^\dagger - \Gamma_{i_1, i_2'}^\dagger),$$

$$S_{i_1, i_3'}^{eff} = - \tau e^{i\Lambda} \frac{\rho^2}{1 + \alpha^2} (\Gamma_{i_1, i_3'}^\dagger + \alpha^2 \Gamma_{i_1, i_3'}^\dagger),$$

$$S_{i_1, i_3'}^{eff} = \tau e^{i\Lambda} \frac{\alpha \rho^2}{1 + \alpha^2} (\Gamma_{i_1, i_3'}^\dagger - \Gamma_{i_1, i_3'}^\dagger). \quad (\text{A2})$$

Having (A2) available we easily obtain the remaining 30 elements of  $\hat{S}^{eff}$  based on symmetry and Eq. (13).

<sup>10</sup>The value of  $H_0$  is proportional to the squared interband gap; the parameter  $\alpha$  is equal to the absolute value of the ratio of the nondiagonal (with respect to band number) matrix elements of the electron velocity operator. Both quantities are calculated at  $k_M$ .

<sup>20</sup>The authors thank D. A. Fushman for providing the simplex-method algorithm used here.

<sup>1</sup>M. H. Cohen and L. M. Falicov, Phys. Rev. Lett. **7**, 231 (1961).

<sup>2</sup>R. W. Stark and L. M. Falicov, Progr. Low Temp. Phys. **5**, 735 (1967).

<sup>3</sup>M. I. Kaganov and A. A. Slutskin, *Conduction Electrons* Nauka, Moscow (1985).

<sup>3b</sup>A. A. Slutskin, Zh. Eksp. Teor. Fiz. **53**, 767 (1967) [Sov. Phys. JETP, **26**, 474 (1967)].

<sup>4</sup>D. Schanberg, *Magnetic Oscillations in Metals*, Mir, Moscow (1986).

<sup>5</sup>N. E. Alekseevskiy and V. I. Nizhankovskiy, *Conduction Electrons*, Nauka, Moscow (1985).

<sup>6</sup>Yu. N. Proshin, Zh. Eksp. Teor. Fiz. **93**, 1356 (1987) [Sov. Phys. JETP **66**, 770 (1987)].

<sup>7</sup>L. M. Falicov, A. B. Pippard, and P. R. Sievert, Phys. Rev. **151**, 498 (1966).

<sup>8</sup>M. H. Cohen and E. I. Blount, Phil. Mag. **5**, 115 (1960).

<sup>9</sup>J. Jafet, Sol. St. Phys. **14**, 1 (1963); G. L. Bir and G. E. Pikus, *Symmetry and Strain-Induced Effects in Semiconductors*, Wiley, New York (1975).

<sup>10</sup>R. W. Stark, Phys. Rev. **135A**, 1968 (1964).

<sup>11</sup>Yu. N. Proshin and N. Kh. Usetnov, Fiz. Tverd. Tela. **32**, 935 (1990) [Sov. Phys. Solid State, **32**, 552 (1990)].

<sup>12</sup>I. M. Lifshits, M. Ya. Azbel' and M. I. Kaganov, *Electron Theory of Metals*, Consultants Bureau, New York (1973).

<sup>13</sup>A. A. Abrikosov, *Fundamentals of the Theory of Metals*, North-Holland, Amsterdam (1988).

<sup>14</sup>*Handbook of Mathematical Functions*, M. Abramovits and I. M. Stigan (Eds.), Natl. Bur. Standards, Govt. Printing Office, Washington, DC (1964).

<sup>15</sup>E. C. Sowa and L. M. Falicov, Phys. Rev. B **32**, 755 (1985); J. K. Freericks and L. M. Falicov, Phys. Rev. B **39**, 5678 (1989).

<sup>16</sup>S. P. Cracknell, *The Fermi Surface*, Clarendon, Oxford (1973).

<sup>17</sup>A. B. Pippard, Proc. Roy. Soc. A. **287**, 165 (1965).

<sup>18</sup>A. A. Slutskin, Zh. Eksp. Teor. Fiz. **58**, 1098 (1970) [Sov. Phys. JETP, **31**, 589 (1970)]; Zh. Eksp. Teor. Fiz. **65**, 2114 (1978) [Sov. Phys. JETP, **38**, 1057 (1974)].

<sup>19</sup>A. J. Bennett and L. M. Falicov, Phys. Rev. A **136**, 998 (1964).

<sup>20</sup>J. P. Van Dyke, J. W. McClure, and J. F. Doar, Phys. Rev. B **1**, 2511 (1970).

<sup>21</sup>F. A. Buot, R. L. Li, and J. O. Strom-Olsen, J. Low Temp. Phys. **22**, 535 (1976).

Translated by Kevin S. Hendzel